RSC Advances

PAPER

View Article Online
View Journal | View Issue

Cite this: *RSC Adv.*, 2020, **10**, 8207

Efficient and stable catalyst of α-FeOOH for NO oxidation from coke oven flue gas by the catalytic decomposition of gaseous H_2O_2†

Ziheng Meng,[ab] Chenye Wang,[a] Xingrui Wang[a] and Huiquan Li *[ab]

Received 18th January 2020
Accepted 12th February 2020

DOI: 10.1039/d0ra00533a

rsc.li/rsc-advances

Goethite (α-FeOOH) possesses excellent catalytic activity, high selectivity and good stability as a catalyst for NO oxidation through the catalytic decomposition of gaseous H_2O_2. $HO_2^{\bullet}/O_2^{\bullet-}$ as the primary reactive oxygen species is involved in the NO oxidation process together with ·OH, and N_2O_5 is found for the first time in the products of NO oxidation.

Sulphur dioxide (SO_2) and nitrogen oxides (NO_x) yielded by fossil fuels and ore combustion are the major air pollutants produced by traditional chemical industries, including iron and steel, coking, and boilers, and these pollutants cause acid rain, fog, and haze. Wet flue gas desulphurisation (WFGD) and selective catalytic reduction (SCR) are efficient methods used in power plants for desulphurisation and denitration, respectively.[1] However, in traditional chemical industries, for example, coke oven flue gas yielded by coke oven gas combustion has a flue gas temperature of about 200–230 °C and the composition is complex,[2] which limits the utilisation of SCR.[3]

Recently, we proposed a promising process of gas-phase oxidation combined with wet scrubbing using steel slag slurry to treat NO_x from low-temperature flue gas.[4,5] In this process, the sparingly soluble NO could be oxidised into soluble NO_2, HNO_3 or N_2O_5 through the gas-phase oxidation process, and then the oxidation products could be absorbed together with SO_2 in a wet scrubbing device. This method can achieve the simultaneous removal of SO_2 and NO_x using the oxidisers. Some oxidisers, such as O_3,[6,7] H_2O_2,[8–12] $NaClO_2$,[13] NaClO,[14] persulphate salt ($S_2O_8^{2-}$)[15] and ferrate (Fe[VI]),[16] can be used as the gas-phase oxidiser for NO oxidation after being gasified if needed.

H_2O_2 is a green and low-cost oxidizer, which can be used as the gas-phase oxidizer for NO oxidation after liquid H_2O_2 is gasified at low temperature. Furthermore, the oxidation potential of H_2O_2 (1.77 eV) is lower compared with that of O_3 (2.08 eV) and ·OH (2.80 eV) and thus its efficiency in oxidising NO is low.[12,17] Thermal decomposition of gaseous H_2O_2 can decompose H_2O_2 into radicals (·OH or $HO_2^{\bullet}/O_2^{\bullet-}$) with high oxidation potential for NO oxidation. However, this technology requires high H_2O_2 consumption (H_2O_2/NO = 80) and excessive residence time (34 s) and results in low NO oxidation efficiency (~60%).[18] Introducing catalysts into the H_2O_2 decomposition process can effectively decompose H_2O_2 into radicals and considerably reduce the consumption of H_2O_2.[11] Iron-based materials, such as hematite (α-Fe_2O_3),[8] nanoscale zero-valent iron,[9] Fe_3O_4,[10] γ-Fe_2O_3@Fe_3O_4,[11] $Fe_2(MoO_4)_3$ [19] and $Fe_2(SO_4)_3$,[12] have been used as catalysts to decompose gaseous H_2O_2 for NO oxidation. These catalysts have high removal efficiencies as heterogeneous catalysts for the simultaneous removal of NO and SO_2 in an integrated catalytic oxidation/wet scrubbing process. However, the use of these catalysts results in relatively high H_2O_2 consumption[8,9,12,20] and relatively low gas hourly space velocity (GHSV)[19] and catalytic stability.[9,12] Therefore, a catalyst with low H_2O_2 consumption and high GHSV and catalytic stability for NO oxidation through catalytic decomposition of gaseous H_2O_2 should be developed.

Goethite (α-FeOOH) is a ubiquitous natural mineral in soils and sediments at the Earth's surface that is widely used as a heterogeneous Fenton catalyst for wastewater treatment due to its abundance, availability, relative stability and low cost.[21] He *et al.* explored the catalytic performance of α-FeOOH and found that it can be used to catalyse H_2O_2 vapour for NO oxidation under low-temperature (<160 °C) flue gas;[22] however, coke oven flue gas has a higher flue gas temperature (200–230 °C), and the reaction products and catalytic mechanism may be different under different temperature regions. Therefore, the performance of α-FeOOH for NO oxidation through catalysing gaseous H_2O_2 under high flue gas temperature should be investigated, and the SO_2 oxidation efficiency of this process should also be evaluated. Herein, NO and SO_2 conversions and NO_2 yield using α-FeOOH with gaseous H_2O_2 were performed under the wide temperature range of 100–350 °C, and the catalytic stability and reaction mechanism were determined.

[a]*CAS Key Laboratory of Green Process and Engineering, National Engineering Laboratory for Hydrometallurgical Cleaner Production Technology, Institute of Process Engineering, Chinese Academy of Sciences, Beijing 100190, China. E-mail: hqli@ipe.ac.cn*

[b]*School of Chemical Engineering, University of Chinese Academy of Sciences, Beijing 100049, China*

† Electronic supplementary information (ESI) available. See DOI: 10.1039/d0ra00533a

Fresh α-FeOOH catalyst was prepared *via* precipitation reaction of Fe^{3+} followed by crystal transformation according to the method of Böhm.[23] All chemicals used in the experiments were of analytical grade, and deionised water was used. NO, NO_2, and SO_2 concentrations in simulated flue gas were analysed using a UV differential optical absorption spectroscopy (DOAS) flue gas comprehensive analyser (Laoying3023, Qingdao Laoying Environmental Technology Co., Ltd.). The presence of HNO_3 and N_2O_5 in the flue gas were detected using a Fourier transform infrared (FTIR) spectrometer (Tensor 27, Bruker Optik, Inc.), which was equipped with a 2.4 m gas cell. Catalysts were characterised *via* X-ray diffraction (XRD) spectroscopy (Empyrean, PANalytical Instruments) and FTIR spectrometry. Hydroxyl radical (·OH) and superoxide anion radical ($HO_2^{\cdot}/O_2^{\cdot-}$) decomposed by H_2O_2 were detected *via* electron paramagnetic resonance (EPR) spectroscopy (A300-10/12, Bruker Optik Inc.), and 5,5-dimethyl-1-pyrroline *N*-oxide (DMPO) was used for capturing ·OH and $HO_2^{\cdot}/O_2^{\cdot-}$. Specifically, DMPO–$H_2O$ solvent was used to capture the ·OH generated after H_2O_2 was catalysed, whereas DMPO–CH_3OH was used to capture $HO_2^{\cdot}/O_2^{\cdot-}$. The experimental equipment for evaluating the catalytic performance of α-FeOOH was established (Fig. S1, ESI†). In brief, the bypass of N_2 carried the gaseous H_2O_2 generated by the evaporation of H_2O_2 solution and mixed with the simulated flue gas, and then the mixture gas contacted with the catalyst, in which gaseous H_2O_2 was decomposed into radicals over the catalyst and oxidised NO and SO_2. At the outlet of the catalytic reactor, the simulated flue gas after being oxidised was detected using a UV DOAS flue gas comprehensive analyser and an FTIR spectrometer equipped with a gas cell. Each experiment was conducted for 20 min after the temperature was stabilised.

According to Christensen *et al.*, α-FeOOH is transformed to hematite (α-Fe_2O_3) within the temperature range of 171–311 °C, and α-FeOOH is totally converted to α-Fe_2O_3 at 350 °C.[24] The fresh catalyst and the catalyst calcinated at 350 °C were characterised *via* XRD and FTIR spectrometry. The FTIR and XRD spectra (Fig. S2 and S3, ESI†) indicated that the fresh catalyst was α-FeOOH and the catalyst calcinated at 350 °C was α-Fe_2O_3 in an N_2 atmosphere. The colour of the fresh catalyst (yellow) and the calcinated catalyst (red) also proved the above results (Fig. S4, ESI†). An FTIR spectrometer equipped with a gas cell was used to analyse the water vapour and further investigate the transformation temperature of α-FeOOH. Results (Fig. S5, ESI†) showed that α-FeOOH began to decompose into α-Fe_2O_3 and H_2O when the temperature was above 200 °C in an N_2 atmosphere. However, when H_2O(g) and H_2O_2(g) were existed in N_2 atmosphere, they could improve the thermal stability of α-FeOOH. The reason may be that (1) multiple types of surface hydroxyls (–OHs) generated by the adsorption of water on α-FeOOH surface prevented the dehydration of –OHs;[25,26] and (2) H_2O(g) from the injected H_2O_2 solution were adsorbed on the reduced ≡Fe(II) and generated ≡Fe(II)–OH *via* eqn (1) and (2), and ≡Fe(II)–OH was converted to ≡Fe(III)–OH *via* eqn (3).[12,19,22,27,28] The catalyst α-FeOOH was still stable when temperature was up to 225 °C, and little α-FeOOH close to the wall of the reactor was converted to α-Fe_2O_3 (the color of catalyst was changed from yellow to red) when temperature was up to 350 °C. Therefore, the catalyst α-FeOOH possesses great thermal stability under the simulated flue gas condition (*e.g.*, the experimental condition in Fig. 1).

$$\equiv Fe(III) + H_2O_2 \rightarrow \equiv Fe(II) + HO_2^{\cdot} + H^+ \quad (1)$$

$$\equiv Fe(II) + V_o + H_2O \rightarrow \equiv Fe(II)\text{–}OH_2^+ \rightarrow \equiv Fe(II)\text{–}OH + H^+ \quad (2)$$

$$\equiv Fe(II)\text{–}OH + H_2O_2 \rightarrow \equiv Fe(III)\text{–}OH + \cdot OH \quad (3)$$

As shown in Fig. 1, NO conversion and NO_2 yield were both lower than SO_2 conversion when gaseous H_2O_2 only was used for NO oxidation. This result indicated that SO_2 was more easily oxidised by gaseous H_2O_2 than NO, which consumed a large amount of H_2O_2. NO conversion and NO_2 yield were higher, but SO_2 conversion was considerably lower than using gaseous H_2O_2 only when α-FeOOH was used to catalyse gaseous H_2O_2 for NO oxidation. Therefore, α-FeOOH performed excellent catalytic activity and high selectivity for NO oxidation. Specifically, NO conversion achieved 98.8% and NO_2 yield reached 77.0% at H_2O_2/NO of 2.0, reaction temperature of 225 °C, catalyst dosage of 0.5 g and GHSV of 137 747 h^{-1}. The catalyst of α-FeOOH achieved a higher NO oxidation efficiency under low H_2O_2 consumption and high GHSV compared with those reported by previous studies (Table S1, ESI†).[8,9,12,17,19,20]

Fig. 1 shows that NO conversion was higher than NO_2 yield within the temperature range of 100–225 °C, and NO conversion was closer to NO_2 yield when the temperature further increased from 250 °C to 350 °C. This trend indicated that the products of NO oxidation was not just NO_2 within the temperature range of 100–225 °C, and the product of NO oxidation might only be NO_2 within the temperature range of 250–350 °C. The products of NO oxidation were determined *via* FTIR spectroscopy. As shown in Fig. 2, the peaks for NO_2 (1599 cm^{-1}), HNO_3 (886 cm^{-1}) and N_2O_5 (1719 cm^{-1}) were observed in the FTIR spectra within the temperature range of 100–200 °C.[29,30] However, no obvious peaks for NO_2, HNO_3, and N_2O_5 were detected in the FTIR spectra when H_2O_2 was not added. This result indicated that

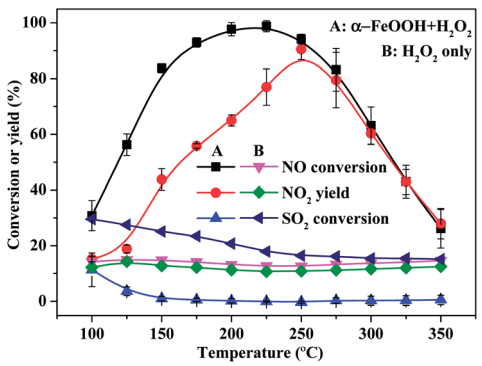

Fig. 1 Effects of temperature on NO and SO_2 conversions and NO_2 yield (H_2O_2/NO, 2.0; H_2O_2 solution feeding rate, 148.9 μL min^{-1}; catalyst dosage, 0.5 g; GHSV, 137 747 h^{-1}; NO concentration, 200 ppm; SO_2 concentration, 660 ppm; O_2 concentration, 6%).

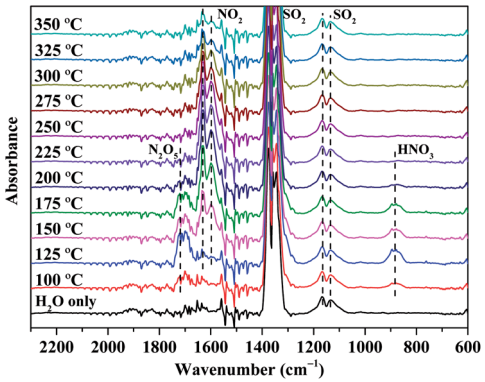

Fig. 2 FTIR spectra of simulated flue gas oxidised by gaseous H_2O_2 over α-FeOOH under different temperature conditions. (Experimental condition was the same as that in Fig. 1.)

NO_2, HNO_3 and N_2O_5 were the main products of NO oxidation through the catalytic decomposition of gaseous H_2O_2 over α-FeOOH in low-temperature (100–200 °C) region. Furthermore, the peaks for HNO_3 and N_2O_5 in the FTIR spectra disappeared when the temperature increased from 225 °C to 350 °C. The reason is that HNO_3 and N_2O_5 decomposed in the high-temperature region (225–350 °C) (eqn (4) and (5)).[29] In summary, NO_2, HNO_3 and N_2O_5 were the main products of NO oxidation in the low-temperature region (100–200 °C), whereas NO_2 was the main product in the high-temperature region (225–350 °C).

$$N_2O_5 \rightarrow NO + NO_2 + O_2 \quad (4)$$

$$2HNO_3 \rightarrow NO + NO_2 + O_2 + H_2O \quad (5)$$

Fig. 1 shows that NO conversion sharply increased when the temperature increased from 100 °C to 200 °C and then decreased when the temperature further increased from 225 °C to 350 °C. The increase in NO conversion with temperature was because high temperatures enhance H_2O_2 decomposition into radicals according to the Arrhenius law,[12] which further accelerates NO conversion. The decrease in NO conversion at temperatures above 200 °C could be explained by (1) the thermal decomposition of gaseous H_2O_2 under high temperature and/or (2) the transformation of α-FeOOH under high temperature. On the one hand, gaseous H_2O_2 can be decomposed under high temperature. An FTIR spectrometer equipped with a gas cell was used to detect gaseous H_2O_2 under different temperature conditions (free of catalyst) to investigate the decomposition temperature of gaseous H_2O_2,[31] and the variations in H_2O_2 content were measured by their homologous infrared absorption characteristic peaks (Fig. S6, ESI†). Results (Fig. S7, ESI†) indicated that H_2O_2 almost did not decompose at 100–300 °C, and the thermal decomposition of gaseous H_2O_2 occurred when the temperature increased further to 300 °C. On the other hand, NO-TPD (Fig. S8, ESI†) showed that the absorbed NO began to desorb when the temperature was above 200 °C. Therefore, when the temperature was above 200 °C, NO conversion decreased when the temperature was above 200 °C. Overall, the transformation of α-FeOOH under high temperature (>200 °C) led to the decrease in NO conversion when the temperature was above 200 °C, and the thermal decomposition of gaseous H_2O_2 also resulted in the decrease in NO conversion when the temperature was above 300 °C.

The catalytic stability of α-FeOOH was also investigated. As shown in Fig. 3, NO conversion was maintained at a high level (>97.0%) within the first 15 h and then fluctuated slightly but remained at >90.0% at 15–45 h. SO_2 conversion remained stable at about 2.0%. Results indicated that α-FeOOH possesses excellent catalytic activity, good stability and high selectivity for NO oxidation. According to the results in Fig. 1 and 3, the catalyst has an ideal temperature window of 175–250 °C; therefore, α-FeOOH can be applied in coke oven flue gas (200–230 °C) treatment.

Fresh and used (after the 45 h test) α-FeOOH were characterised *via* FTIR and XRD spectroscopy. The bands at 3363, 3127 and 1628 cm^{-1} are the O–H stretching mode in α-FeOOH, the stretching mode of surface water and the bending mode of H_2O, respectively. The characteristic strong bands at 795 and 891 cm^{-1} were assigned to the Fe–O–H bending vibrations of α-FeOOH. The band at 638 cm^{-1} was assigned to the Fe–O stretching vibration of pure α-FeOOH. The characteristic absorption peaks of α-FeOOH in the catalyst after the 45 h test did not change compared with that of the fresh catalyst (Fig. S9, ESI†), indicating that the catalyst maintained the structure of α-FeOOH even after the 45 h test. The band at 999 cm^{-1} was assigned to $\nu_1(SO_4)$ frequency, and the bands at 1076, 1136 and 1229 cm^{-1} were interpreted as $\nu_3(SO_4)$ frequencies. These vibrational frequencies are attributed to specifically adsorbed SO_4^{2-} ions on the external and internal surfaces of catalyst particles after the 45 h test.[32,33] The XRD patterns showed that the phase of the catalyst before and after the stability test was still α-FeOOH (Fig. S10, ESI†). This result also indicated that α-FeOOH possessed good stability in the NO oxidation process.

EPR test was conducted to detect the radicals generated by H_2O_2 decomposition and analyse the oxygen species of the α-FeOOH/H_2O_2 system. Fig. 4 shows the 4-fold characteristic peak

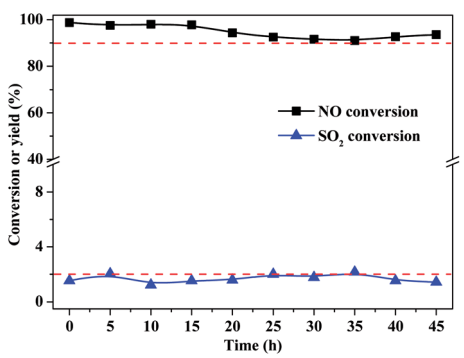

Fig. 3 Catalytic stability of α-FeOOH. (H_2O_2/NO, 2.0; H_2O_2 solution feeding rate, 148.9 μL min^{-1}; catalyst dosage, 0.5 g; GHSV, 137 747 h^{-1}; temperature, 225 °C; NO concentration, 200 ppm; SO_2 concentration, 660 ppm; O_2 concentration, 6%.)

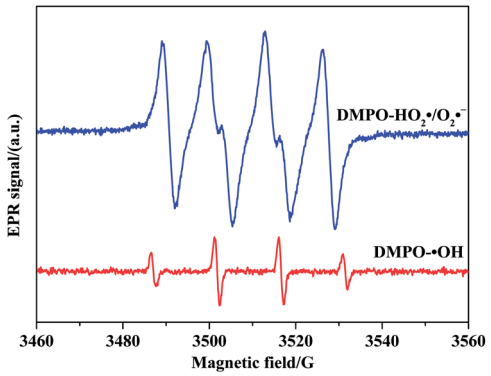

Fig. 4 EPR spectra of the α-FeOOH/H_2O_2 system.

of DMPO–·OH adducts with an intensity ratio of 1 : 2 : 2 : 1 and four notable signals ascribed to DMPO – $HO_2^{\bullet}/O_2^{\bullet-}$ adducts. These peaks and signals indicate the formation of ·OH and $HO_2^{\bullet}/O_2^{\bullet-}$ in the α-FeOOH/H_2O_2 system.[21,34] Furthermore, the intensity of the 4-fold characteristic peak of DMPO–·OH adducts was significantly weaker than that of DMPO – $HO_2^{\bullet}/O_2^{\bullet-}$ adducts, indicated that the quantity of $HO_2^{\bullet}/O_2^{\bullet-}$ produced by the α-FeOOH/H_2O_2 system was larger than that of ·OH. Therefore, α-FeOOH can decompose H_2O_2 into ·OH and $HO_2^{\bullet}/O_2^{\bullet-}$, and $HO_2^{\bullet}/O_2^{\bullet-}$ may be dominant among ·OH and $HO_2^{\bullet}/O_2^{\bullet-}$ for NO oxidation. Radical trapping experiments (Fig. S11, ESI†) further proved the roles of radicals (·OH and $HO_2^{\bullet}/O_2^{\bullet-}$) in the NO oxidation process. Benzoquinone (BQ, $HO_2^{\bullet}/O_2^{\bullet-}$ scavenger[20]) was added into the H_2O_2 solutions, and H_2O_2 and BQ in the mixture solution was vapoured together. NO conversion substantially decreased from 92.9% to 6.1% when the molar ratio of BQ to H_2O_2 increased from 0 to 1.0. The reason was that the addition of BQ captured the $HO_2^{\bullet}/O_2^{\bullet-}$ generated by gaseous H_2O_2 decomposition over α-FeOOH, thereby decreasing NO conversion. NO conversion decreased from 92.9% to 8.0% when isopropanol (i-PrOH, ·OH scavenger[20]) was introduced into the same system as the molar ratio of i-PrOH to H_2O_2 increased from 0 to 8.0. The reason was that ·OH generated in the α-FeOOH/H_2O_2 system was captured by i-PrOH instead of oxidised NO. These results indicated that when the addition concentration of the ·OH scavenger (i-PrOH) was eight times that of $HO_2^{\bullet}/O_2^{\bullet-}$ scavenger (BQ), both systems obtained the similar decrease in NO conversion. Therefore, $HO_2^{\bullet}/O_2^{\bullet-}$ as the primary reactive oxygen species was involved in the NO oxidation process together with ·OH.

In this catalytic process, the reaction between H_2O_2 as an oxidant and iron ions as a catalyst to produce highly active species (·OH and $HO_2^{\bullet}/O_2^{\bullet-}$).[35] The conversion between Fe^{2+} and Fe^{3+} was proceed according to the Haber–Weiss mechanism. ≡Fe(III)–OH and ≡Fe(III) are reduced by H_2O_2 and generate ≡Fe(II)–OH and ≡Fe(II) (eqn (6) and (1)), the resulting ≡Fe(II)–OH and ≡Fe(II) also can be oxidized by H_2O_2 and produce ≡Fe(III)–OH and ≡Fe(III) (eqn (3) and (7)).[12,19,22,27,28,36]

$$\equiv Fe(III)-OH + H_2O_2 \rightarrow \equiv Fe(II)-OH + HO_2^{\bullet} \quad (6)$$

$$\equiv Fe(II) + H_2O_2 \rightarrow \equiv Fe(II) + \cdot OH + OH^- \quad (7)$$

The proposed mechanism of NO oxidation by H_2O_2 decomposition over α-FeOOH is presented in Fig. 5 based on the study of the products of NO oxidation and reactive oxygen species ($HO_2^{\bullet}/O_2^{\bullet-}$ and ·OH) in the NO oxidation process. (1) Gaseous H_2O_2 decomposed into ·OH and $HO_2^{\bullet}$ on the active sites (≡Fe(II)–OH and ≡Fe(II), ≡Fe(III)–OH and ≡Fe(III)) of the catalyst (eqn (1)–(3), (6) and (7)) according to the Haber–Weiss mechanism, a result that was proved through EPR analysis and scavenger experiments. (2) NO was oxidised by the generated ·OH and $HO_2^{\bullet}$ and produced NO_2 and HNO_3 *via* eqn (8) and (9). (3) The produced HNO_3 reacted with ·OH and produced NO_3 or NO_2 (eqn (10) and (11)). (4) NO_2 reacted with NO_3 and produced N_2O_5 *via* eqn (12).[37] The production of NO_2, HNO_3 and N_2O_5 during the NO oxidation process was proved by the FTIR spectra (Fig. 2).

$$NO + 2\cdot OH \rightarrow NO_2 + H_2O \quad (8)$$

$$NO + HO_2^{\bullet} \rightarrow HNO_3 \quad (9)$$

$$HNO_3 + \cdot OH \rightarrow NO_3 + H_2O \quad (10)$$

$$HNO_3 + \cdot OH \rightarrow NO_2 + H_2O_2 \quad (11)$$

$$NO_2 + NO_3 \rightarrow N_2O_5 \quad (12)$$

In summary, α-FeOOH can be used as an efficient catalyst for coke oven flue gas to enhance NO oxidation efficiency through the catalytic decomposition of gaseous H_2O_2. Moreover, α-FeOOH showed high selectivity for NO oxidation in the presence of SO_2. In this study, NO conversion achieved 98.8% under the following experimental conditions: H_2O_2/NO of 2.0, reaction temperature of 225 °C, catalyst dosage of 0.5 g and GHSV of 137 747 h^{-1}. The 45 h test indicated that α-FeOOH has good catalytic stability. The EPR test and radical trapping experiments revealed that $HO_2^{\bullet}/O_2^{\bullet-}$ as the primary reactive oxygen species was involved in the NO oxidation process together with ·OH. Furthermore, NO_2, HNO_3 and N_2O_5 were the products of

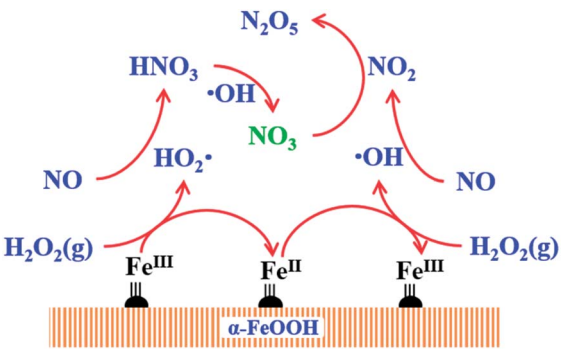

Fig. 5 Catalytic mechanism of NO oxidation by H_2O_2 decomposition over α-FeOOH (≡Fe^{III}:≡Fe(III), ≡Fe(III)–OH; ≡Fe^{II}:≡Fe(II), ≡Fe(II)–OH).

NO oxidation through the catalysis of gaseous H_2O_2 over α-FeOOH within the temperature range of 100–200 °C, and NO_2 was the only oxidation product within the temperature range of 225–350 °C.

The catalyst α-FeOOH can be used to decompose gaseous H_2O_2 into radicals and oxidise NO into high-valence NO_x, and then the oxidation products can be absorbed together with SO_2 in existing industrial-scale WFGD systems.[4,5] This process can achieve the simultaneous removal of SO_2 and NO_x from coke oven flue gas.

Conflicts of interest

There are no conflicts of interest to declare.

Acknowledgements

This work was financially supported by the NSFC (51574214) and the Young Scientists Fund of the NSFC (21706264).

Notes and references

1 A. J. Sweeney and Y. A. Liu, *Ind. Eng. Chem. Res.*, 2001, **40**, 2618–2627.
2 H. Yin, W. Lü, G. Sun, G. Sun and B. Hong, *Fuel & Chemical Processes*, 2015, **46**, 1–4.
3 Q. Ma, Z. Wang, F. Lin, M. Kuang, R. Whiddon, Y. He and J. Liu, *Energy Fuels*, 2016, **30**, 2302–2308.
4 Z. Meng, C. Wang, X. Wang, Y. Chen and H. Li, *Energy Fuels*, 2018, **32**, 2028–2036.
5 Z. Meng, C. Wang, X. Wang, Y. Chen, W. Wu and H. Li, *Fuel*, 2019, **255**, 115760.
6 J. Zhang, R. Zhang, X. Chen, M. Tong, W. Kang, S. Guo, Y. Zhou and J. Lu, *Ind. Eng. Chem. Res.*, 2014, **53**, 6450–6456.
7 S. Zhou, J. Zhou, Y. Feng and Y. Zhu, *Ind. Eng. Chem. Res.*, 2016, **55**, 5825–5831.
8 B. Wu, Y. Xiong, J. Ru and H. Feng, *Korean J. Chem. Eng.*, 2016, **33**, 3407–3416.
9 Y. Zhao, B. Yuan, R. Hao and Z. Tao, *Energy Fuels*, 2017, **31**, 7282–7289.
10 S. Yang, Y. Xiong, Y. Ge and S. Zhang, *Mater. Lett.*, 2018, **218**, 257–261.
11 S. Yang, Y. Xiong and S. He, *ChemistrySelect*, 2019, **4**, 8829–8836.
12 B. Wu, Y. Xiong and Y. Ge, *Chem. Eng. J.*, 2018, **331**, 343–354.
13 Y. Zhao, R. Hao, B. Yuan and J. Jiang, *J. Hazard. Mater.*, 2016, **301**, 74–83.
14 Y. Zhao, R. Hao, F. Xue and Y. Feng, *J. Hazard. Mater.*, 2017, **321**, 500–508.
15 R. Hao, X. Wang, X. Zhao, M. Xu, Y. Zhao, X. Mao, B. Yuan, Y. Zhang and K. Gao, *Chem. Eng. J.*, 2018, **333**, 583–593.
16 Y. Zhao, Y. Han, T. Ma and T. Guo, *Environ. Sci. Technol.*, 2011, **45**, 4060–4065.
17 B. Wu and Y. Xiong, *J. Chem. Technol. Biotechnol.*, 2018, **93**, 43–53.
18 K. Kou, W. Zhou, Y. Wang, H. Zhao and J. Gao, *Can. J. Chem. Eng.*, 2019, **97**, 2419–2425.
19 X. Liu, C. Wang, T. Zhu, Q. Lv, Y. Li and D. Che, *Chem. Eng. J.*, 2019, **371**, 486–499.
20 B. Yang, S. Ma, R. Cui, S. Sun, J. Wang and S. Li, *Chem. Eng. J.*, 2019, **359**, 233–243.
21 H. Jin, X. Tian, Y. Nie, Z. Zhou, C. Yang, Y. Li and L. Lu, *Environ. Sci. Technol.*, 2017, **51**, 12699–12706.
22 S. He, Y. Xiong, S. Yang and Y. Ge, *Chem. Ind. Eng. Prog.*, 1–12, DOI: 10.16085/j.issn.1000-6613.2019-0630.
23 J. Böhm, *Z. Anorg. Allg. Chem.*, 1925, **149**, 203–216.
24 A. N. Christensen, T. R. Jensen, C. R. H. Bahl and E. DiMasi, *J. Solid State Chem.*, 2007, **180**, 1431–1435.
25 G. Bbuscå and P. F. Rossi, *Mater. Chem. Phys.*, 1983, **9**, 561–570.
26 J. Jin, Master, Zhengzhou University, 2019.
27 J. Ding, Q. Zhong, S. L. Zhang, F. J. Song and Y. F. Bu, *Chem. Eng. J.*, 2014, **243**, 176–182.
28 J. Ding, Q. Zhong and S. L. Zhang, *J. Mol. Catal. A: Chem.*, 2014, **393**, 222–231.
29 C. L. Sun, N. Zhao, Z. K. Zhuang, H. Q. Wang, Y. Liu, X. L. Weng and Z. B. Wu, *J. Hazard. Mater.*, 2014, **274**, 376–383.
30 H. J. Yoon, H.-W. Park and D.-W. Park, *Energy Fuels*, 2016, **30**, 3289–3297.
31 M. Pettersson, S. Tuominen and M. Räsänen, *J. Phys. Chem. A*, 1997, **101**, 1166–1171.
32 S. Musić, Z. Orehovec, S. Popović and I. Czakó-Nagy, *J. Mater. Sci.*, 1994, **29**, 1991–1998.
33 K. Kandori, T. Shigetomi and T. Ishikawa, *Colloids Surf., A*, 2004, **232**, 19–28.
34 D. Huang, J. Li, G. Zeng, W. Xue, S. Chen, Z. Li, R. Deng, Y. Yang and M. Cheng, *Chem. Eng. J.*, 2019, **375**, 121991.
35 S. R. Pouran, A. A. A. Raman and W. M. A. W. Daud, *J. Cleaner Prod.*, 2013, **64**, 1–12.
36 L. Guo, Q. Zhong, J. Ding, M. Ou, Z. Lv and F. Song, *Ozone: Sci. Eng.*, 2016, **38**, 382–394.
37 Z. Wen, PhD, Zhejiang University, 2009.